Rayleigh scattering on a microwave surfatron plasma to obtain axial profiles of the atom density and temperature

Eur. Phys. J. Appl. Phys. (2012) 58: 20802
DOI: 10.1051/epjap/2012110294

THE EUROPEAN PHYSICAL JOURNAL
APPLIED PHYSICS

Regular Article

Rayleigh scattering on a microwave surfatron plasma to obtain axial profiles of the atom density and temperature

S. Hübner[a], E. Iordanova, J.M. Palomares, E.A.D. Carbone, and J.J.A.M. van der Mullen

Department of Applied Physics, Eindhoven University of Technology, 5600 MB Eindhoven, The Netherlands

Received: 25 July 2011 / Received in final form: 17 February 2012 / Accepted: 16 April 2012
Published online: 25 May 2012 –

Abstract. The axial dependency of the central-axis value of the heavy particle density and temperature of surface-wave plasmas is studied using Rayleigh scattering (RyS). The plasma is generated at a frequency of 2.45 GHz in argon by a surfatron operating under the standard settings of a power of 45 W, a flow rate of 50 sccm and a pressure of 20 mbar. To investigate the effect of the pressure on the gas temperature, we also investigated 6 and 10 mbar plasmas. By using a two-dimensional intensified CCD array we could determine and eliminate the influence of false stray light, a major disturbing factor in the determination of the Rayleigh signal. In order to trace the energy fluxes that determine the gas temperature, we performed Thomson scattering so that the properties of the electron gas are known. It is found that the gas temperature, T_a, depends on the wall temperature and the product of the gas pressure and the electron pressure. The latter implies that T_a follows the electron density axially, meaning that it is highest at the launcher and decreases monotonically in the wave propagation direction. The maximum gas temperature of around $T_a = 800$ K is found close to the launcher for the highest gas pressure of 20 mbar. For lower pressures we find lower T_a values. The extrapolation of T_a toward the end of the plasma column leads to a temperature of about 320 K. This study reveals that, for the argon plasmas under study, the central-axis values of the gas temperature are determined by the balance between the heating of the gas by means of elastic electron collisions and the cooling due to heat conduction from the center to the wall.

1 Introduction

Surface-wave discharges (SWDs) form a special type of microwave induced plasmas that have been studied and investigated systematically [1–3]. Due to their broad range of operating conditions, stability and reproducibility, they have received many technological applications. In order to further improve these applications, insight into plasma parameters and mechanisms is needed. A well-known method, in the field of low pressure SWDs, of classifying plasma parameters is to use "similarity laws". These make it possible to translate plasma properties of known conditions into those of plasma conditions that have not been investigated yet.

This study is initiated by the application of SWDs for the production of optical fibers [4,5]. These plasmas are operated in the range of intermediate pressures, that is around a pressure of $p = 20$ mbar. Plasmas created in this pressure range can generate high radical fluxes while the pressure is sufficiently low to avoid constriction and filamentation. In contrast to the low pressure SWDs there are not so many studies performed for the intermediate pressure range. The application or extrapolation of similarity laws found for the low pressure plasmas to this class of plasmas is not a priori justified.

In many experimental and theoretical methods a lot of attention is paid to the properties of the free electrons $\{e\}$; see for instance [6] where the electron density n_e and the electron temperature T_e are determined using Thomson scattering (TS). However, in an atomic plasma of low ionization degree the main plasma constituent is the ground-state atom. The density and temperature of the atoms, hereafter denoted by n_a and T_a, are connected to each other by the pressure $p = n_a k_B T_a$, a control parameter that is easy to measure. This implies that only one of the parameters n_a or T_a has to be determined if p is known.

The knowledge of n_a or T_a is important for instance in the experimental method of absolute line intensities (ALI). The ground-state density compared to the density of the excited radiating species gives the electron temperature by employing a collisional radiative model [7]. The measurement of the continuum of atomic plasmas can give the electron density [8,9]. In the case that the degree of ionization is small, the atoms are the main scatter partners of the electrons so that again the n_a value is needed for a correct interpretation of the continuum spectrum.

Also in modeling plasmas, n_a is an essential parameter [10,11]. It is an important factor for the reduced

[a] e-mail: s.huebner@tue.nl

electric field (E/n_a), and for the determination of the rate of elastic and inelastic collisions. Therefore, n_a is needed for a proper understanding of the plasma heating and the creation of light and radicals.

In the literature several methods can be found to measure n_a or T_a. Generally they can be divided as based on emission spectroscopy [12], laser absorption spectroscopy [12–15] and laser scattering [16]. In case of emission spectroscopy the T_a can for instance be obtained from the rotational temperature of excited molecular species. A disadvantage of applying this method to atomic plasmas is that an addition of molecules is required and that this can change the plasma properties substantially.

In references [17,18] the T_a is derived from the Doppler width of the absorption transition 4s → 4p in argon. This method, for which a tuneable narrow band laser is needed, gives line-of-sight information. Just as in the case of emission spectroscopy one needs methods, like the Abel inversion procedure, to convert the lateral spectral profiles into spatially resolved temperatures.

In this work, we determine the main gas properties using Rayleigh scattering (RyS); a method familiar to TS in the sense that both, TS and RyS, are related to the elastic scattering of photons on electrons. In the case of TS the electrons are free whereas in the case of RyS they are bound. One of the big advantages of laser-scattering techniques is that they directly provide spatially resolved information since only photons generated in the small intersection volume of the optical axis and the laser beam are detected. Another advantage of laser-scattering techniques is that direct information is obtained of the plasma parameter under study.

For the RyS measurements we use a similar setup as that used for TS measurements [6]. They are performed on surfatron induced plasmas in argon at intermediate pressure; the frequency is fixed at 2.45 GHz. The standard conditions are an absorbed power of 45 W, an argon gas flow of 50 sccm and a gas pressure of 6, 10 or 20 mbar.

Surfatron induced plasmas (SIPs) belong to the class of surface-wave produced plasmas with the common feature that, since the wave loses energy while traveling along the plasma column, the electron density decreases in the wave propagation direction. This implies that the heat transfer from electrons $\{e\}$ to the heavy particles $\{h\}$ will also decrease in the wave propagation direction. The precise knowledge of this process is of importance for a proper understanding for these types of plasmas. Therefore, the knowledge of the behavior of n_a (or T_a) along the discharge column is indispensable and it should be measured together with the properties of the electron gas, n_e and T_e.

The current study can be seen as an extension of the work reported in reference [19] on RyS measurements performed in our laboratory on a SWD delivered by a group from Orsay (Paris-Sud). There are three essential differences:

(i) We apply RyS to a plasma with a much smaller radius (3.0 mm versus 8.0 mm) implying that it is much more difficult to handle false stray light (FS); i.e., the light generated by the scattering of the laser (side-beams) on dust particles or the wall. However, since we use a 2D iCCD array instead of a 1D photo-diode array in the detection system as in reference [19], we get better insight into the role and strength of FS.

(ii) Our RyS scattering experiments are done in conjunction with TS so that apart from the properties of $\{h\}$ also n_e and T_e are obtained. In this way we can trace the energy flow from $\{e\}$ to $\{h\}$. In reference [19] the properties of the electron gas were not known.

(iii) In the current work we observe different axial positions of a plasma operated at a constant power whereas in reference [19] the observed position is fixed (7 cm from the gap) while the power is changed. To get the gas temperature as a function of the axial position, the study in reference [19] relied upon a similarity law that states that the properties of plasmas of the same pressure, radius and composition only depend on the distance to the end of the column (DEC).

The results found in reference [19] based on the DEC-similarity law raised some questions. The shape of the axial dependence of the central values of the T_a was found to be composed of two branches: a constant (plateau) value close to the launcher and a steep decay close to the plasma end. The presence of this plateau is in contradiction with the fact that plasma power density gradually decreases along the discharge.

It is the aim of the current study to investigate the energy balance of the heavy particles in more detail. As we know the features of the electron gas (from TS) we can compute the heat transfer from electrons to heavy particles, balance that with heat conduction and compare the resulting T_a values with the result of RyS. In both the TS and RyS methods we will not rely upon similarity laws and measure n_e, T_e and T_a on different axial positions of one and the same plasma; that means that we keep the control parameters and especially the power constant.

This DEC-similarity law used in reference [19] originating from the practice of low pressure SWDs and applied to intermediate pressure SWDs is not the only law that is questionable. In Section 4 we will, just as in our previous study [6], find that the T_e-similarity law that relates the T_e to the product n_aR of the gas density n_a and plasma radius R is also not valid for the plasmas under study.

This paper is organized as follows: Section 2 gives a theoretical background by comparing RyS with TS. Section 3 describes the experimental setup and experimental procedure for RyS measurements followed by an error analysis. The results are presented and discussed in Sections 4 and 5. Finally, Section 6 provides concluding remarks.

2 Theory of RyS and TS

Laser scattering can deliver substantial information about the main plasma parameters such as the temperature of the electrons and the densities of the electrons and heavy particles. The interpretation of the experimental results is

rather straightforward and does not depend on the degree of equilibrium departure. Moreover, the methods are non-intrusive, provided the laser power is not too high [20].

The scattering of (laser-)photons on free electrons is known as Thomson scattering and on bound electrons we speak of as Rayleigh (or Raman) scattering. The fact that RyS and TS have much in common implies that the same setup initially developed for TS [6,21,22] can also be employed for RyS. Only minor adjustments are needed (cf. Sect. 3). The same applies for the theoretical treatment which will be given here.

The spectral power $P_\lambda^x(\Delta\Omega)$ of the scattered radiation collected in the solid angle element $\Delta\Omega$ reads:

$$P_\lambda^x(\Delta\Omega) = P_\mathrm{i} n_x L S_\lambda(\lambda)\Delta\Omega \frac{\mathrm{d}\sigma^x}{\mathrm{d}\Omega}. \quad (1)$$

Here, P_i is the incident laser power, L is the length over which the observed laser-medium interaction takes place, n_x is the density of the scattering particles, $\mathrm{d}\sigma^x/\mathrm{d}\Omega$ is the differential cross-section while $S_\lambda(\lambda)$ contains the spectral information. We assume that $S_\lambda(\lambda)$ is normalized, meaning that $\int S_\lambda(\lambda)\mathrm{d}\lambda = 1$. In the case of TS the spectral information comes from the thermal motion of free electrons, $S_\lambda(\lambda)$ can be resolved and gives the electron temperature.[1] In the case of RyS this is not possible (with our setup) since the thermal velocity of the heavy particles is much smaller. We can only work with the spectral integrated form of equation (1) which, using the normalization of $S_\lambda(\lambda)$, gives:

$$P_\lambda^x(\Delta\Omega) = P_\mathrm{i} n_x L \Delta\Omega \frac{\mathrm{d}\sigma^x}{\mathrm{d}\Omega}. \quad (2)$$

This expression can be used to obtain both n_e and n_a by inserting the corresponding value of $\mathrm{d}\sigma^x/\mathrm{d}\Omega$.

The relative importance of RyS with respect to TS can be determined by comparing the product of the gas density and differential Rayleigh cross-section with the corresponding product for TS. This gives:

$$\frac{P^\mathrm{RyS}}{P^\mathrm{TS}} = \frac{(n_\mathrm{a}\mathrm{d}\sigma^\mathrm{a}/\mathrm{d}\Omega)}{(n_\mathrm{e}\mathrm{d}\sigma^\mathrm{e}/\mathrm{d}\Omega)} = 6.8\times10^{-3} n_\mathrm{a}/n_\mathrm{e}, \quad (3)$$

where we inserted the value $\mathrm{d}\sigma^\mathrm{e}/\mathrm{d}\Omega = 7.94\times10^{-30}\ \mathrm{m^2\ sr^{-1}}$ for TS (for 90° of observation and polarization) and for RyS on argon $\mathrm{d}\sigma^\mathrm{a}/\mathrm{d}\Omega = 5.4\times10^{-32}\mathrm{m^2 sr^{-1}}$ for $\lambda_\mathrm{i} = 532$ nm. Note that the differential cross-section $\mathrm{d}\sigma^\mathrm{a}/\mathrm{d}\Omega$ for RyS strongly depends on λ whereas the differential cross section of TS is wavelength independent.

In both RyS and TS cases we apply a double perpendicular scattering arrangement meaning that the detection takes place in a direction at 90° to the incident laser beam while the polarization is perpendicular to the plane formed by the laser and the detection direction.

Equation (3) shows that for typical ionization ratios of about $n_\mathrm{e}/n_\mathrm{a} = 10^{-4}$ for the plasmas under study, the strength of RyS is about 70 times stronger than that of TS. Thus, it is advised to remove RyS during TS measurements. Since RyS is generated within a small spectral band around the laser wavelength λ_i, this removal can be done by using a notch filter centered around λ_i.

If RyS is the study objective, a notch filter makes no sense since we are interested in the photons at, and in the immediate vicinity of, the laser wavelength. However, apart from the RyS the signal will contain false stray (FS) light as well, so that extra precautions must be taken to reduce the generation of FS and to find a method to disentangle RyS signal from FS.

The above information also makes it clear that RyS measurements can be performed in a much shorter measurement time than TS. A typical TS measurement needs 20 min, while for RyS this is around 2 min.

3 Experimental setup and settings

3.1 The experimental setup

The experimental setup (cf. Fig. 1) consists of three main parts: the laser setup (on the left), the plasma tube (bottom right) and the detection system (top right). Since the setup was discussed in previous publications [6,21,22], we will only mention the main changes and give the information that is needed to make this paper self-contained. For the laser we used an Edgewave class IV that produces laser pulses at 532 nm with a repetition rate of 5 kHz, a duration of 10 ns and energy content of 4 mJ. This replaces the laser in reference [6], where the repetition rate was 10 Hz, while the pulse energy was typically 100 mJ.

This means that with the present setup the number of collected photons per unit of time is 20 times larger.

The measurements have been performed on microwave induced argon surfatron plasmas. The EM waves are generated by a magnetron, that can deliver a maximum power of 200 W at a fixed frequency of 2.45 GHz. The generated plasma is confined in a quartz tube with inner and outer radii of $r_{inner} = 3.0$ mm and $r_{outer} = 4.0$ mm, respectively. Brewster windows are attached on both sides of the tube to minimize laser reflections and to assure maximum transmission. The argon pressure can be controlled by mass flow controllers and is measured by two pressure meters.

An essential feature of this setup is that the plasma tube can be translated along its own axis. During this translation the central axis remains coincident with the laser beam and a new axial plasma position is brought into the spatial fixed detection volume. In this way we can investigate the central-axis values of the plasma properties n_e, T_e, n_a and T_a as a function of axial position without changing the plasma control parameters. So, there is no need to rely upon the DEC-similarity law that states that we can get another less (more) energetic plasma location by keeping the distance of the detection volume to the launcher fixed while decreasing (increasing) the power.

[1] In the plasmas under study the TS is non-collective meaning that the electrons respond individually to the laser light (cf. Refs. [6,21,22]).

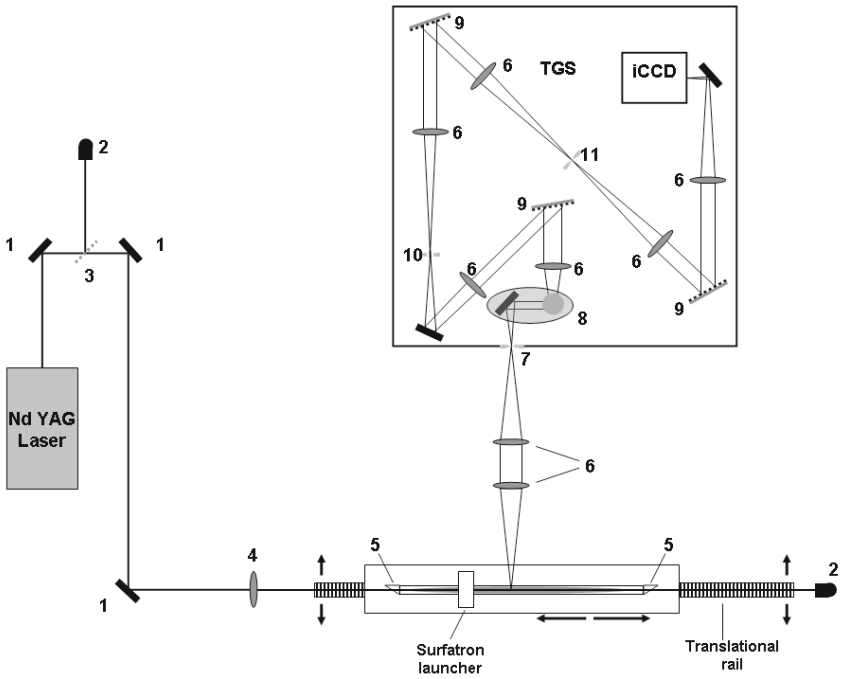

Fig. 1. Schematic view of the setup showing the threefold structure of the setup: laser (left), plasma source (bottom) and detection branch (top). The horizontal bold arrows along the plasma tube indicate that it can be translated along its own axis; an essential feature of this setup. The numbered components have the following meaning: 1 – 45° mirror; 2 – beam dump; 3 – beam splitter; 4 – 1 m plano-convex lens; 5 – Brewster window; 6 – achromatic lens; 7 – entrance slit; 8 – image rotator; 9 – grating; 10 – mask; 11 – intermediate slit.

The scattered light is collected by an optical system of two parallel lenses that focuses the photons onto the entrance slit of a triple grating spectrograph (TGS). The TGS had been designed [21,23] with the purpose to reject the false stray light and Rayleigh scattered photons and to disperse and collect the remaining TS signal. The combination of the first two gratings and the mask in the middle forms a notch filter, whereas the final dispersion is performed by the third grating that sends the dispersed image to an iCCD. In the present study the setup is used to perform both TS and RyS. Changing from one to the other can be done by simply (re)placing or removing the mask between the first two gratings (cf. Fig. 1). By removing the mask the function of the notch filter is switched off.

The emitted plasma signal is collected by a two-dimensional iCCD camera giving spectral information in the horizontal and spatial information in the vertical direction. Each iCCD frame covers a plasma (or gas) length of 1.2 cm. A pixel binning process can be applied in spatial and spectral directions in order to reduce the noise and smooth the spectra.

Figure 2 compares two iCCD images. The upper frame shows the TS signal, the lower the RyS+FS signal. The number of shots, given in the frames, shows that much less TS than RyS+FS photons are collected per unit of time; therefore, the central wavelength must be blocked, i.e., the notch filter must be in function, for the detection of TS photons. The TS spectrum is much broader so that it can deliver the T_e value. In the lower frame the notch filter is "switched off" so that the scattering photons with λ values around the central wavelength of 532 nm are collected. The vertical signal strip gives a mixture of photons generated by RyS and FS. Apart from the "glow-like" regions also "spots" can be seen. These are the result of laser scattering on dust particles, small impurities carried by the gas flow and deposited on the wall tube. Since the laser is very intense and the tube radius with 3 mm rather small, there is a reasonable chance that one of the laser side-beams interacts with one of these particles. It is very important to choose zones from the central signal strip that are free of false stray light. These dust-breakfree zones are selected for the determination of the FS level.

In Figure 2 an example of four different glow regions is given; they are bound by four pairs of horizontal lines. By bringing the pressure to the lowest possible value we reduce RyS so that only the FS is left. This is subsequently subtracted from the mixed spectrum of RyS+FS under plasma condition. We stress the fact that this exploration of the RyS and FS signal and the elimination of strong FS zones is a novel technique that is based on the benefit of working with a 2D iCCD. In the experiment reported in reference [19] use was made of a 1D iphoto-diode array. Apart from the fact that an iCCD is much more sensitive it can also be used to study the composition of RyS and FS by iCCD-picture inspection.

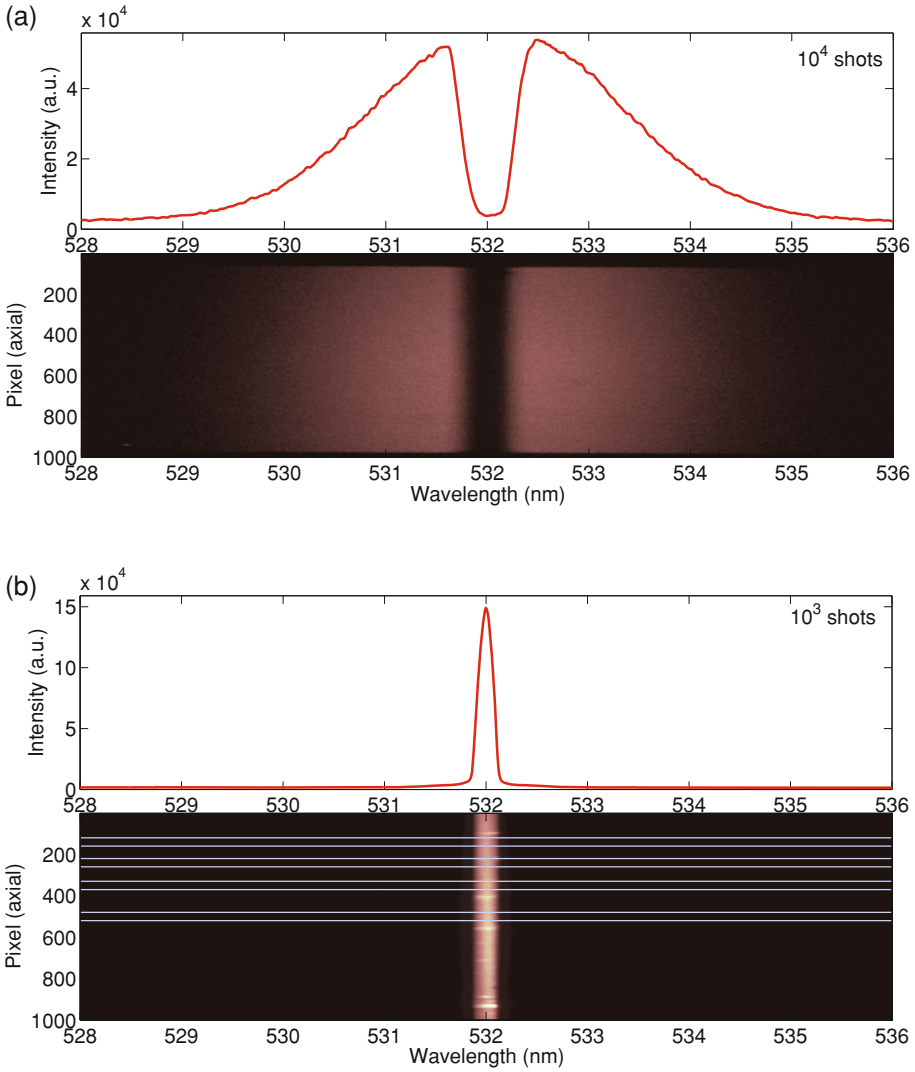

Fig. 2. (Color online) Typical iCCD images of TS (a-bottom) and RyS+FS (b-bottom) and the corresponding spectral profile (a-top and b-top); the horizontal direction corresponds to the wavelength dispersion while the vertical direction gives the position along the beam-medium interaction zone; the 1000 pixels in that direction correspond to 1.2 cm. The iCCD TS frame (a-bottom) shows that the central wavelength is blocked (notch filter "switched on"); this is done in order to avoid overexposure due to RyS+FS. The TS spectral profile (a-top) is obtained after vertical binning (spatial direction). In the lower iCCD frame (b-bottom) the notch filter is "switched off" so that the scattering around the central wavelength of 532 nm can be collected; the central strip shows that apart from the "glow-like" regions also spots can be seen. The four pairs of horizontal lines mark glow regions that are free of spots; the spectral profile shown above (b-top) is obtained after binning all these "spot-free" regions vertically.

3.2 Determination of the heavy particle density

For the TS procedure we refer to reference [6], where the axial dependence of TS and the associated determination of n_e and T_e are given for comparable plasma conditions. Here we confine ourselves to the description of the RyS procedure.

The RyS measurements consist of three steps.

(i) In the first step RyS is performed on a plasma with a known gas pressure. This gives a signal with RyS and FS components, hereafter denoted by $S(\mathrm{RyS}_{\mathrm{plasma}} + \mathrm{FS})$.

(ii) The second measurement is done on an argon flow at room temperature. The plasma is off while the pressure and thus $n_a(\mathrm{gasfill}) = p/k_B T_{\mathrm{room}}$ is known. The signal of this measurement is denoted by $S(\mathrm{RyS}_{\mathrm{gasfill}} + \mathrm{FS})$.

(iii) The third measurement is again with plasma off but now under vacuum conditions; the signal is supposed to be equal to the signal of the FS and denoted by $S(\mathrm{FS})$.

In all the three steps the same number of shots (with the same energy per pulse) is applied. The signal $S(\mathrm{FS})$ of the third step can be subtracted from the signal obtained in the first and second steps giving the RyS for the plasma and room temperature Ar gas. Employing equation (2)

on both the plasma and room temperature and taking the quotient, we can eliminate the factor $P_i L(\mathrm{d}\sigma/\mathrm{d}\Omega)\Delta\Omega$. This gives the relation:

$$\frac{n_a(\text{plasma})}{n_a(\text{gasfill})} = \frac{S(\text{RyS}_{\text{plasma}} + \text{FS}) - S(\text{FS})}{S(\text{RyS}_{\text{gasfill}} + \text{FS}) - S(\text{FS})}, \quad (4)$$

from which n_a (plasma) can be determined since n_a (gasfill), the density of the gas at room temperature, can be determined using the ideal gas law and the known gas pressure.

Note that the RyS method gives, just as in the case of TS, radial-resolved results since only photons generated in the intersection region of the laser beam and the optical axis of the detector optics are detected. This gives insight into the axial properties of the plasmas, more precisely for the region of 250 μm around $r = 0$.

3.3 The experimental procedure

The experimental procedure starts with aligning the plasma tube along the laser beam. Not only the tube but the whole surfatron supporting table has to be positioned correctly. So by translating the table the volume observed by the TGS remains at the same position in the laboratory frame but changes position in the plasma frame.

Another aspect of the alignment is that the detection volume is focused onto the entrance slit of the TGS. The detection volume has a size of 1.2 cm along the laser beam and a width of 250 μm. The former is the length of the iCCD frame, the latter the width of the slit.

After the alignment, the discharge tube is filled with argon gas and the plasma is launched. The gas pressure and gas flow are settled at the desired values. Hereafter the three steps given above can be performed so that we get for the position and condition in question the values of the triplet $S(\text{RyS}_{\text{plasma}} + \text{FS})$, $S(\text{RyS}_{\text{gasfill}} + \text{FS})$ and $S(\text{FS})$.

For a new set of measurements the plasma table is translated so that the detection branch is focused onto a different plasma position. If necessary, minor radial realignments can be done. The discharge can now be reignited under the same pressure and power conditions, and a new triplet of RyS measurements can be performed.

3.4 The error analysis

The largest error in the RyS method comes from the false stray light FS. The impact of this error source on the final quantities n_a and T_a will be analyzed using equation (4), which for convenience is denoted here as $Q = N/D$, while the signal and the absolute error in FS will be denoted by F and ΔF.

First, we look at errors in the numerator $N = S(\text{RyS}_{\text{plasma}} + \text{FS}) - S(\text{FS})$, where indeed FS plays an important role as it contributes to both signals. As stated above we determine the $S(\text{FS}) \equiv F$ from the "spot-free" zones in the central iCCD strip. This is done with the aim to reduce ΔF. Figure 2 gives an example from which we could deduce that the relative error typically equals $\Delta F/F = 7\%$. Since the *absolute* error in $S(\text{RyS}_{\text{plasma}} + \text{FS})$ is more or less equal to ΔF, we find for the absolute error in N that $\Delta N = \sqrt{2}\Delta F$.

To determine the relative error in N, we first express the Ry signal in terms of F by introducing the ratio $\xi = S(\text{RyS}_{\text{plasma}} + \text{FS})/S(FS)$. This means that $N \approx (\xi - 1)F$ and thus that the error due the subtraction leads to $\Delta N/N \approx (\sqrt{2}/(\xi - 1))(\Delta F/F)$. For the relative error in the denominator $D = S(\text{RyS}_{\text{gasfill}} + \text{FS}) - S(\text{FS})$ we find accordingly $\Delta D/D = (\sqrt{2}/(\varsigma - 1))(\Delta F/F)$ where we introduced the parameter $\varsigma = S(\text{RyS}_{\text{gasfill}} + \text{FS})/S(\text{FS})$. Putting things together leads to:

$$\frac{\Delta Q}{Q} = \frac{\Delta F}{F}\sqrt{\frac{2}{(\xi - 1)^2} + \frac{2}{(\varsigma - 1)^2}}. \quad (5)$$

For the 20 mbar case it was found that $\xi \approx 2$ while ς is larger. Taking $\Delta F/F = 7\%$ and the worst-case scenario of $\xi = \varsigma$, we find that $\Delta Q/Q = 2\Delta F/F = 14\%$. It should be realized that the errors in the lower pressure cases of $p = 6$ and 10 mbar will be larger. The reason is that ξ will be smaller under these conditions.

This error caused by the FS is much larger than any other error source such as the error related to the fluctuation of the laser power, the plasma reproducibility and the reading of the pressure meter. So, the limitation of this method is determined by the beam quality of the laser. For the investigation of plasmas of lower pressures one needs a laser of high beam purity. However, for low pressure conditions gas heating is not an important phenomenon.

4 Results

Figure 3 gives the atom density n_a as a function of axial position. The position $z = 0$ corresponds to the exit of the launcher while the direction of increasing z is that of the surface-wave propagation. The end point of the plasmas is in all cases denoted by signs corresponding to the pressure legend. The plasmas were all operated at an absorbed power of 45 W. Apart from the standard condition of 20 mbar, we also give the result for two different pressures, namely 6 and 10 mbar.

Figure 4 gives the corresponding T_a values as a function of the distance z. We see that in the case of 20 mbar the highest gas temperature value of about $T_a = 800$ K is measured at the closest position to the launcher exit. For $p = 6$ mbar the highest value is about 500 K. The reason for this pressure dependence of T_a is, globally, that for high n_a values the heat exchange between electrons and atoms is higher while the heat conductivity is n_a-independent. We come back to that in the discussion part below. Note that the extrapolation of T_a toward the end of the plasma column leads in all cases to a temperature of about 310 K which is close to room temperature; as should be. In contrast with the work published in reference [19] we do not see a plateau in the launcher region.

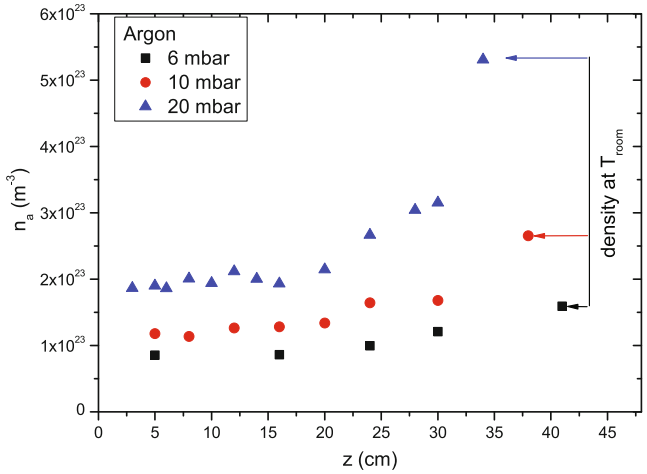

Fig. 3. (Color online) Axial profiles of the n_a for the gas pressures of 6, 10 and 20 mbar, absorbed MW power of 45 W, mean laser power of 12 W and an argon gas flow of 50 sccm.

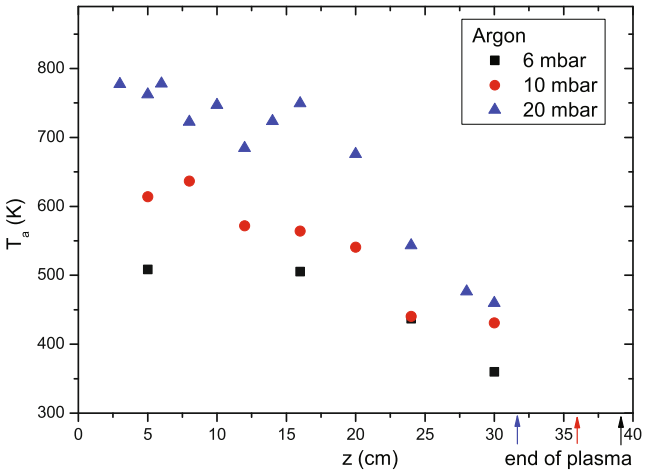

Fig. 4. (Color online) Axial profiles of the gas temperature T_a for the same conditions as those of the previous figure.

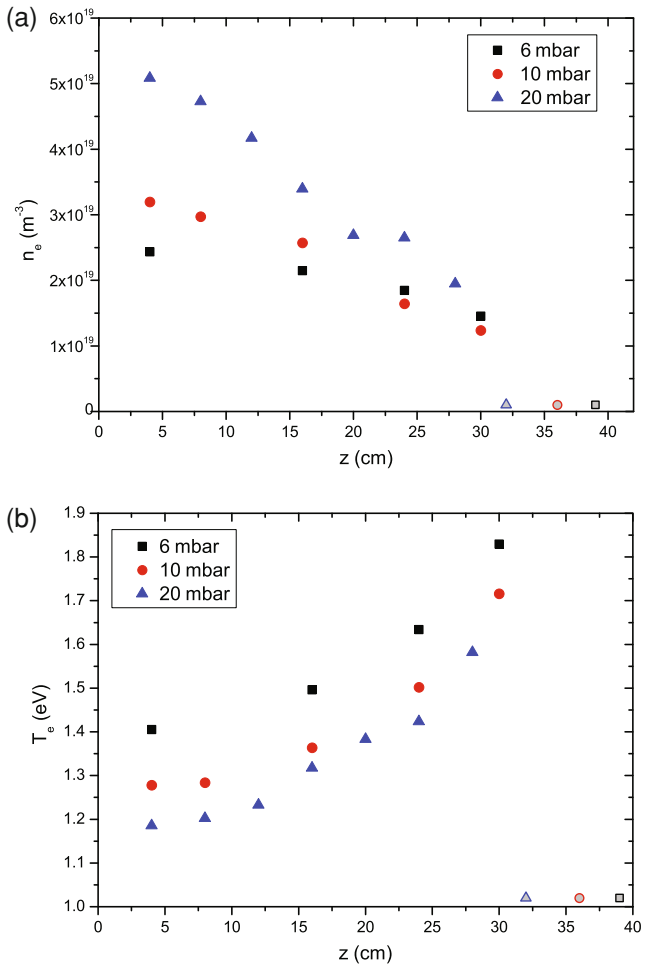

Fig. 5. (Color online) The electron density n_e (5a) and temperature T_e (5b) as functions of the axial position obtained with TS experiment for three different pressures; the plasma settings are the same as those corresponding to Figures 3 and 4. The signs on the right bottom side point to the end of the plasma column; they correspond to the pressure legend.

According to that work the axial dependence of the central value of the gas temperature consists of two branches: the first one is more or less constant, thus a plateau, the second branch is a steep slope in T_a in the region close to the plasma end. As pointed out in reference [19] the presence of the plateau is in contradiction with the fact that the plasma power density decreases monotonically along the wave propagation direction.

The temperature of the gas is determined by the energy flow:

$$EM \rightarrow \{e\} \rightarrow \{h\} \rightarrow \text{environment}$$

showing that the electrons receive energy from the EM field and pass that over to the heavy particles. These in turn transfer their heat to the environment.

Thus, for a proper understanding of the plasma heating and the resulting gas temperature T_a we should know the properties of the electron gas $\{e\}$ at each relevant axial position. For that purpose we performed TS measurements.

The results presented in Figures 5a and 5b giving n_e and T_e show the same trends as those reported in reference [6] where they are discussed extensively. Here we give a brief summary.

- The central-axis value of n_e decreases almost linearly in the wave propagation direction with a slope that depends on the pressure.
- Extrapolation of the found axial n_e curve toward the visual plasma end gives an n_e value that is much larger than the critical density n_c. The latter is obtained by equating the plasma frequency to frequency of the exciting wave; numerically it equals $n_c = 3.5{\times}10^{17}$ m^{-3}.
- The T_e values close to the launcher were found to fit reasonably with the results predicted by the electron particle balance (ePB), which supports the observed trend that an increase in pressure leads to a decrease in T_e. The ePB is the basis of the T_e-similarity law that states that plasmas (or plasma slabs) with the same

value of $n_a R$ have the same electron temperature. This law is indeed valid in the region close to the launcher for which we can see that (just as the product $n_a R$) T_e is almost constant.

- However, it is found that T_e gradually increases in the wave propagation direction, thus in the direction of decreasing n_e. Increases of about 30% over 30 cm were found. In the discussion given in reference [6] we attributed this violation of the T_e-similarity law to the deviation of the electron energy distribution from the Maxwellian equilibrium form. This is in line with the studies [11,12,25].

Note that the accuracy in n_e and T_e obtained by TS is quite high. The random errors in both quantities are less than 3% and smaller than the errors resulting from the fluctuations in the laser pulse energy and the plasma non-reproducibility. This high-level accuracy can be reached since, due to the notch filter, the determination of the TS signal is not hindered by FS.

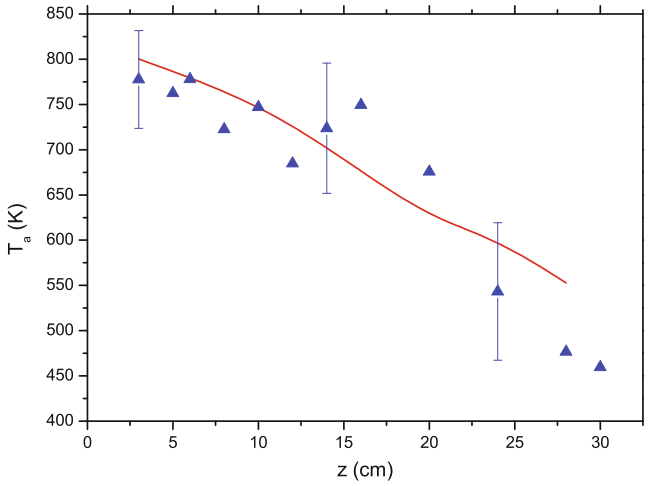

Fig. 6. (Color online) Comparison of T_a values derived from the experimental RyS (triangles) measurements at 20 mbar and the calculation (line) based on equations (6)–(8).

5 Discussion

The gas temperature in the plasma is determined by the energy balance of the heavy particles. This balance equates the heat transfer from the electrons to the heavy particles to the cooling of the heavy particles by the surroundings. The following assumptions are made:

(i) the pressure is constant along the axis,
(ii) convective heat transport can be neglected,
(iii) inelastic energy transfer from electrons to heavy particles is unimportant,
(iv) the mechanism of sheath heating does not affect the central value of T_a,
(v) the rate coefficient for the heat transfer from electrons to heavy particles is constant along the radius.

Under these assumptions the energy balance reads:

$$n_e n_a S_{heat} k_B (T_e - T_a) = -\nabla \times (\lambda_h \nabla T_a), \qquad (6)$$

where k_B is Boltzmann's constant and λ_h is the thermal conduction coefficient. The coefficient of heat transfer S_{heat} is related to that of electron-atom momentum transfer S_{mom} by means of $S_{heat} = (3m_e/M)S_{mom}$, where m_e and M are the masses of the electron and the argon atom, respectively. Since $T_e \gg T_a$, we may use $T_e - T_a = T_e$. Substituting $n_a = p/k_B T_a$ equation (6) turns into:

$$S_{heat} p_e p = \frac{\lambda_h k_B (T_a - T_W) T_a}{R^{*2}}, \qquad (7)$$

where T_W is the wall temperature, $p_e = n_e k_B T_e$ the electron pressure, whereas R^* is the thermal diffusion length, a distance comparable to the radius of the plasma tube. To arrive at this equation we neglected the radial dependence of λ_h, p_e and S_{heat} and replaced the differential operations by dividing by the radius twice. This resulting expression is a quadratic equation for T_a with solution:

$$T_a = \frac{T_W}{2}(1 + (1 + 4C(p_e p)/T_W^2)^{1/2}), \qquad (8)$$

where $C = S_{heat}(k_B \lambda_h)^{-1} R^{*2}$. This solution shows that the axial temperature depends on a competition between the wall temperature T_W and the product of the pressures of the electrons and heavy particles $p_e p$. The dependence on the gas pressure can be seen (cf. Fig. 4) by comparing the T_a values at the launcher for different p values. The highest T_a value is obtained at the highest pressure of 20 mbar. The reason basically is that for increasing n_a the transfer between electrons and heavy particles (lhs of Eq. (6)) will increase whereas the heat conduction (rhs) is n_a independent. The dependence on the electron pressure is manifest in the decay of T_a along the axis. Along the wave propagation direction p_e goes down and as a consequence the heavy particles will receive less heat.

Figure 6 gives a comparison between the T_a values obtained from equation (8) and experiments. We inserted the n_e and T_e values obtained from TS measurements (cf. Fig. 5). Since n_e values are for $r = 0$, we divided the value by 1.64 assuming a Bessel-like profile. For the value of C, we used $R^* = 3$ mm, $\lambda_h = 0.0178$ W(mK)$^{-1}$ [26] and $S_{heat} = 6.7 \times 10^{-19}$ m^3 s^{-1} based on the work of references [27–29]. It can be seen that the agreement between theory and experiment is reasonable and falls in between the error bars. Meaning that the T_a values indeed result from the balance between the heating of $\{h\}$ by $\{e\}$ and energy transport. The nature of the first is elastic collision, for the second it is thermal heat conduction.

The validity of the assumptions announced above will be discussed below:

(i) The variation in the pressure was measured experimentally by using two pressure meters, one in the beginning and the other at the end of the tube. A variation was found of $\delta p/p < 1\%$. This can also be supported theoretically by using the Hagen-Poiseuille's law $\delta p = 8L\eta\Phi/\pi r^4$. Taking the standard pressure of $p = 20$ mbar with a flux of $\Phi = 4.2 \times 10^{-5}$ m^3/s (or 50 sccm at 1 bar) argon, the viscosity of argon $\eta = 2 \times 10^{-5}$ Pa s, and the inner tube radius $r_{inner} = 3$ mm,

we find a pressure difference of $\delta p \approx 0.13$ mbar over the $L = 50$ cm long tube. That is less than 1% of the total pressure and thus agrees with the experimental observation.

(ii) The role of convection depends on the term $Q_{\rm conv} = \frac{5}{2}\frac{\partial}{\partial z}(pu)$, where u is the velocity. Since the pressure gradient is small, we can write:

$$Q_{\rm conv} \approx \frac{5}{2} p \frac{\partial}{\partial z} u = \frac{5}{2} p \left(\frac{\Phi}{A}\right)\left(\frac{\Delta T_{\rm a}}{T_{\rm a}}\right), \qquad (9)$$

where A denotes the tube's cross-section. From the experiment we found $\left(\frac{\Delta T_{\rm a}}{T_{\rm a}}\right) < 1$ for all conditions. That results in $Q_{\rm conv} \leq 7 \times 10^3$ Pa/s which can be neglected compared to the radial conduction of $\lambda_{\rm h}(\partial/\partial r)^2 T_{\rm a} \approx 8 \times 10^5$ Pa/s.

(iii) Neglecting inelastic collisions is justified by the fact that internal energy of excited atoms or ions can only be released into translational energy upon interactions with the wall. However, the thermal conductivity of the argon gas compared to the quartz tube is very small; about a factor 70 smaller. This implies that the heat flux due to recombination or quenching at the wall is directed almost completely outward. This can be taken into account by treating the wall temperature as a kind of boundary condition for the heavy particle energy balance.

(iv) The same reasoning applies to the heating due to the plasma sheath. The sheath thickness can be approximated to be about 10 μm. That is rather small compared to the tube radius, which again means that the heat generated in the plasma sheath is conducted outward and does not attribute to the gas heating at the central axis.

(v) Based on reference [30] a constant $T_{\rm e}$ across the radius can be assumed, i.e., $S_{\rm heat}$ can be treated as radially constant.

Topics that should be addressed in future studies are the radial dependence of some quantities like $\lambda_{\rm h}$. That might not be ignored, since $\lambda_{\rm h}$ scales with $T_{\rm a}^{0.5}$ (see Ref. [26] and references therein). To avoid the issues of averaging $\lambda_{\rm h}$, $p_{\rm e}$ and $S_{\rm heat}$, a 1D model should be employed. This will be the subject of further studies.

6 Concluding remarks

To understand the heating mechanism in argon surfatron plasmas at intermediate pressures, we performed Rayleigh scattering experiments for various axial positions. To that end we used a setup in which the plasma can be measured on various positions while the power applied to the plasma remains the same. This, stands in contrast with the method described in reference [19] where plasma regions were shifted by increasing the power so that more energetic plasma parts are brought into the detection volume while increasing the plasma length. This method is based on a popular similarity law that states that for surface-wave discharges (with given pressure and radius) the axial plasma characteristics only depend on the distance to the end of the plasmas and not on the power absorbed by the plasma as a whole.

Another major improvement is that we could use the same setup for the determination of the electron density and temperature using Thomson scattering. In that way we could obtain more precise insight into the heat transfer mechanisms in the plasma that follow a chain in which electrons, accelerated by the field, pass (part of their) heat to the heavy particles that are subsequently cooled by heat conduction to the environment.

In contrast to the work of reference [19], where a steep axial gradient in the gas temperature was found at the end of the plasma column and a nearly constant $T_{\rm a}$ in the bulk plasma we find that the gas temperature decreases gradually in the direction of the wave propagation. This confirms that the gas is heated via the electrons. The central value of the gas temperature is determined by the balance between the heat received from the electrons by means of "elastic" collision and conduction to the wall. Consequently, if the electron pressure is large the heavy particles receive more heat. The gradual decrease of $T_{\rm a}$ along the wave propagation direction is the result of the fact that $p_{\rm e}$ goes down in that direction.

The method can be improved by installing a laser with a better beam quality. In the present setup the laser has side-beams. If one of these hits the wall they will remain propagating in the quartz in much the same way as it happens in a glass fiber. This creates a continuous contribution of background lighting. More seriously is the interaction of the laser with dust particles on the tube. They lead to intense spots on the iCCD images. It is the advantage of the use of a 2D iCCD that due to image inspection these point-like sources can be eliminated in the determination of the pure RyS signal.

The accuracy of the present method is estimated to be 14% for the 20 mbar case. For lower pressures for which the temperature is low, the errors are bigger. However, for our standard condition of 20 mbar, we see that the agreement between theory and experiment is reasonable, which confirms that the heat transfer via elastic electron-atom collisions is responsible for the gas heating.

The method is by no means limited to argon surfatron plasmas and can be employed to other plasma sources and plasma gases. It is interesting to employ the same setup to argon plasmas with admixtures of molecular gases and to investigate how these are changing the heat housekeeping of the plasma. Large changes can be expected since argon is known as a good thermal insulator so that small additions might lead to big changes.

This work was supported by the Dutch Technology Foundation STW Projects 10497 and 10744.

References

1. M. Moisan, J. Pelletier, *Microwave Induced Plasmas, Plasma Technology*, Vol. 4 (Elsevier Science Publishing, The Netherlands, 1992)

2. C.N. Ferreira, M. Moisan, *NATO ASI Series B: Physics*, vol. 302 (Plenum, New York, 1992)
3. H. Schluter, A. Shivarova, Phys. Rep. **443**, 121 (2007)
4. P. Geittner, D. Kuppers, H. Lydtin, Appl. Phys. Lett. **28**, 645 (1976)
5. D. Kuppers, H. Lydtin, *Topics in Current Chemistry* vol. 89 (Springer, Berlin, Heidelberg, 1980), p. 107
6. J.M. Palomares, E. Iordanova, E.M. van Veldhuizen, L. Baede, A. Gamero, A. Sola, J.J.A.M. van der Mullen, Spectrochim. Acta B **65**, 225 (2010)
7. N. de Vries, E. Iordanova, A. Hartgers, E.M. van Veldhuizen, M.J. van den Donker, J.J.A.M. van der Mullen, J. Phys. D: Appl. Phys. **39**, 4194 (2006)
8. E. Iordanova, N. de Vries, M. Guillemier, J.J.A.M. van der Mullen, J. Phys. D: Appl. Phys. **41**, 015208 (2008)
9. E. Iordanova, J.M. Palomares, A. Gamero, A. Sola, J.J.A.M. van der Mullen, J. Phys. D: Appl. Phys. **42**, 0155208 (2008)
10. J. Henriques, E. Tatarova, F.M. Dias, C.M. Ferreira, J. Appl. Phys. **90**, 4921 (2001)
11. T. Petrova, E. Benova, G. Petrov, I. Zhelyazkov, Phys. Rev. E **60**, 875 (1999)
12. A.A. Bol'shakov, B.A. Cruden, S.P. Sharma, Plasma Sources Sci. Technol. **13**, 691 (2004)
13. M. Touzeau, M. Vialle, A. Zellagui, G. Gousset, M. Lefebvre, M. Pealat, J. Phys. D: Appl. Phys. **24**, 41 (1991)
14. A. Rousseau, E. Teboul, N. Sadeghi, Plasma Sources Sci. Technol. **13**, 166 (2004)
15. J.M. Williamson, P. Bletzinger, B.N. Ganguly, J. Phys. D: Appl. Phys. **37**, 1658 (2004)
16. S.C. Snyder, L.D. Reynolds, G.D. Lassahn, J.R. Fincke, C.B. Shaw, R.J. Kearney, Phys. Rev. E **47**, 1997 (1993)
17. E.A.H. Timmermans, Ph.D. Thesis, Eindhoven University of Technology, The Netherlands, 1999
18. J. Jonkers, Ph.D. Thesis, Eindhoven University of Technology, The Netherlands, 1998
19. A. Rousseau, E. Teboul, M.J. van de Sande, J.J.A.M. van der Mullen, Plasma Sources Sci. Technol. **11**, 47 (2002)
20. E.A.D. Carbone, J.M. Palomares, S. Hübner, E. Iordanova, J.J.A.M. van der Mullen, JINST **7**, C01016 (2012)
21. M.J. van de Sande, Ph.D. Thesis, Eindhoven University of Technology, The Netherlands, 2002
22. N. de Vries, J.M. Palomares, W.J. van Harskamp, E. Iordanova, G.M.W. Kroesen, J.J.A.M. van der Mullen, J. Phys. D: Appl. Phys. **41**, 105209 (2008)
23. M.J. van de Sande, J.J.A.M. van der Mullen, J. Phys. D: Appl. Phys. **35**, 1381 (2002)
24. M. Pencheva, T. Petrova, E. Benova, I. Zhelyazkov, J. Phys.: Conf. Ser. **44**, 110 (2006)
25. M. Pencheva, G. Petrov, T. Petrova, E. Benova, Vacuum **76**, 409 (2004)
26. E.W. Lemmon, R.T. Jacobsen, Int. J. Thermophys. **25**, 21 (2004)
27. J.J.A.M. van der Mullen, J. Jonkers, Spectrochim. Acta B **54**, 1017 (1999)
28. H.B. Milloy, R.W. Crompton, J.A. Rees, A.G. Robertson, Aust. J. Phys. **30**, 61 (1977)
29. J. Jonkers, M. van de Sande, A. Sola, A. Gamero, J.J.A.M. van der Mullen, Plasma Sources Sci. Technol. **12**, 30 (2003)
30. E.C. Martinez, Y. Kabouzi, K. Makasheva, M. Moisan, Phys. Rev. E **70**, 066405 (2004)